

Efficient Rectangular Spiral Coil Simulation based on Partial Element Equivalent Circuit Method using Quasistationary Approximation

Manfred Westreicher*, Lukas W. Mayer*, Ralph Prestros[†] and Christoph F. Mecklenbräuer*

* Christian Doppler Laboratory for Sustainable Mobility, Institute of Telecommunications, Vienna Univ. of Technology, Vienna, Austria, email: manfred.westreicher@tuwien.ac.at

[†] NXP Semiconductors Austria GmbH, Gratkorn, Austria

Abstract—We present an efficient method for simulating the impedance of a rectangular spiral coil in the high frequency regime based on the Partial Element Equivalent Circuit (PEEC) method. We use closed form expressions of the corresponding mixed potential integral equation, considering self and mutual inductance as well as capacitance between the elements of a rectangular spiral coil geometry. From the PEEC circuit elements, we abstract an equivalent circuit model that accounts for dominant field interactions. We compare the obtained impedance as a function of frequency with the results of a commercial field solver and benchmark the simulation duration. Our Matlab simulator is by a factor of 8.2 faster, which allows for quick optimization of the spiral coil.

I. INTRODUCTION

Electromagnetic simulation has been widely recognized as a valuable tool for reducing development costs and time to market. In this work, we aim at approximations for the frequency dependent impedance of a rectangular spiral coil from a numerical simulation.

Depending on the problem at hand, different electromagnetic computational techniques are suited better than others, cf. [1] for a survey on this topic. For the case of metal plates and thin wires embedded in homogeneous linear media, the Method of Moments (MoM) has been found particularly suitable. The MoM reduces the functional equation of a linear field problem to a matrix equation, as described in the seminal paper by R.F. Harrington [2].

The Partial Element Equivalent Circuit (PEEC) method is based on the MoM and has been found to be well suited for combined electromagnetic and circuit analysis, as this method models electric and magnetic field interactions as partial resistances, capacitances and inductances, respectively [1]. With this method, conductors are partitioned into basic volume and surface cells with constant current and charge densities. Although the same concept as with PEEC has been used earlier, e.g. [3], the term has been formed by A. Ruehli, who presented the extraction of inductance and capacitance [4], [5] and a survey on the topic [6].

The widely used software packages FastCap [7] and FastHenry [8] are based on circuit parameter extraction using PEEC analysis. The PEEC method can be used for full-wave analysis [9], where time retardation is taken into account, and can be applied to objects with non-orthogonal geometries [10], i.e., where edges of bodies lie not along the axes of the underlying coordinate system. Unfortunately, closed-form solutions of the corresponding integral equations are not available for the full-

wave and non-orthogonal cases, leading to a much higher computational burden and stability issues.

In this work, we focus on a numerically efficient implementation and thus omit time retardation. Conductor geometries are restricted to rectangular cross sections with edges oriented along the axes of the underlying Cartesian coordinate system. For this simple geometry, numerically stable closed-form expressions for the inductances and coefficients of potential exist, allowing for an efficient implementation. Thus, the limitations of the method are the neglected retardation effects and the restricted geometry. The conductors are arranged to form a rectangular spiral coil surrounded by air. The model is extendable to layered dielectric substrates [11].

Our approximation considers only electric interactions of close-by conductors and magnetic interactions of conductors carrying parallel currents, leading to a simplified equivalent coil model consisting of coupled linear network elements. The partitioning of conductors into filaments with small cross section compared to the skin depth squared enables accurate modeling of skin and proximity effects.

The numerically approximated frequency response of the coil impedance is compared to corresponding results obtained by Ansys HFSS Finite Element Method (FEM) solver. The low computational burden of our PEEC based simulator in Matlab is an enabler for the fast optimization for various design goals, e.g., power efficiency, bandwidth or coil dimensions.

The focus lies on coils for Radio Frequency IDentification (RFID) operating in the High Frequency (HF) regime, e.g., in the ISM band around 13.56 MHz, with geometries as described by the international standard ISO/IEC 14443-1 [12]. These coils are typically expensive to analyze with FEM simulations because of their large aspect ratios.

Closely related previous work has been presented in reference [13], where a similar analysis of HF coils was carried out. This work extends [13] to 3D capacitance extraction and we include the coupling of a bridge crossing the coils turns. We introduce a novel equivalent circuit accounting for dominant field interactions. Furthermore, we present accelerated execution of the simulation code including performance comparison with HFSS.

II. COIL ANALYSIS BASED ON MIXED POTENTIAL INTEGRAL EQUATION FORMULATION

The geometry of the approximated coil for testing the simulator is shown in Figure 1. The number of segments is

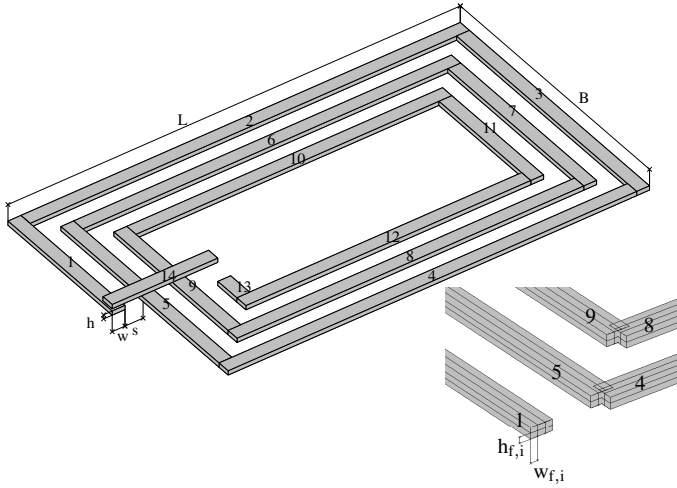


Figure 1. Rectangular spiral coil with tracks of rectangular cross section and corresponding dimensions. Division of segments into filaments with overlap-correction at corners (lower right).

$N_s = 4 \cdot N_t + 2$, with N_t being the number of turns. Each cuboid-shaped segment has an identical rectangular cross sectional area $A = w \cdot h$, where w is the width and h the height of the conductor. Furthermore, two neighbouring segments are separated by distance s . The length l_i of segment i is determined by predefined outer coil dimensions L and B . The unknown charge densities on the conductor surfaces and the current densities within the conductors can be approximated using an integral equation formulation and the Green functional method as shown, e.g., in [14]. In order to model the field interactions due to the currents and charges in form of inductances and capacitances, the conductors are partitioned into volume and surface cells as demonstrated in [14], denoted as filaments and panels in the sequel. Each segment is divided into $N_f = N_w \cdot N_h$ filaments. Similarly as with the segments cross sections, the four lateral boundary surfaces of each segment are divided into $P_w \cdot P_l$ or $P_h \cdot P_l$ panels, respectively, depending on their orientation. Accordingly, the number of panels for the lateral surface of a segment is $N_p = 2 \cdot P_l(P_w + P_h)$. An exemplary division of segments into filaments of width $w_{f,i}$ and height $h_{f,i}$ is shown on the lower right hand side of Figure 1. The cross sectional area and volume of filament i are $A_{f,i} = w_{f,i} \cdot h_{f,i}$ and $V_{f,i} = l_{f,i} \cdot A_{f,i}$, respectively. The area of panel k is denoted $A_{p,k}$. The filaments have cross sectional areas as shown in [13, p.97] and the panels areas are equal for panels residing on the same lateral surface.

As an approximation, we assume free charge to be restricted to the four elongated lateral areas of a segments boundary surface. Furthermore, the current densities are assumed to be constant over the cross section of each filament, and current flow direction is always parallel to the elongated coordinate of the segments. With these simplifications, systematic errors are introduced, especially at the corners where two segments are connected. In order to reduce these errors, the segments

are shifted to overlap at the corners, as shown on the lower right hand side of Figure 1. We argue that with coils where L and B are much larger compared to h and w , these errors will have little effect. Furthermore, the vertical distance between the bridge and the underlying segments is assumed to be small, and no vertical connections (vias) are included in the following PEEC analysis.

The derivation of the Mixed Potential Integral Equation (MPIE) formulation is well known and reported extensively in the literature and therefore omitted in this manuscript, cf. [11]. Since the dimensions of the coils under investigation are much smaller than a tenth of the free space wavelength of our signals of interest, we neglect electromagnetic retardation. Based on the MPIE formulation and the aforementioned discretization of the coils segments into filaments and panels, the field interactions are modeled as partial resistances, inductances and capacitances.

A. Resistance Calculation

The resistance R_i of a filament i made of a material with homogeneous conductivity σ , which has a length $l_{f,i}$ and carries a current density that is constant over its cross section $A_{f,i}$, is calculated by applying Ohm's law as

$$R_i = \frac{l_{f,i}}{\sigma A_{f,i}}. \quad (1)$$

B. Inductance Calculation

In order to determine the outer self inductance L_i of filament i and the mutual inductance $M_{i,j}$ between two filaments i and j , we follow the method presented in [3]. Assuming a homogeneous current density over the cross sections $A_{f,i}$ and $A_{f,j}$ of filaments i and j , the mutual inductance is calculated as

$$M_{i,j} = \frac{\mu}{4\pi A_{f,i} A_{f,j}} \iint \frac{1}{r} dV_{f,i} dV_{f,j} \quad (2)$$

and the self inductance $L_i = M_{i,i}$ is obtained by setting $i = j$. Here, r denotes the Euclidean norm of the position vector of two arbitrary points in the filament(s) and μ is the absolute permeability of air. For the case of parallel conductors with rectangular cross sections, exact analytic expressions of these double volume integrals are given in [3]. Numerical stability of the closed-form expressions was improved by introducing virtual filaments, as shown in reference [15]. Using the results of [15] allows us to calculate the self inductance of each filament and the mutual inductance between two parallel filaments very efficiently.

Since we assume that the magnetic coupling between orthogonal filaments (e.g., filaments from segments 1 and 8 in Fig. 1) due to stray fields being small compared to the parallel case (e.g. filaments from segments 5 and 11 in Fig. 1), these interactions are neglected.

C. Capacitance Calculation

The capacitance between two neighbouring segments is calculated from the coefficients of potential as given in [5]. Assuming a constant charge density on two panels k and l

with areas $A_{p,k}$ and $A_{p,l}$, their mutual coefficient of potential $P_{k,l}$ is calculated as

$$P_{k,l} = \frac{1}{4\pi\epsilon A_{p,k} A_{p,l}} \iint \frac{1}{r} dA_{p,k} dA_{p,l} \quad (3)$$

and the self coefficient of potential is obtained by setting $k = l$. The constant ϵ denotes the absolute permittivity of air and r denotes again the Euclidean norm of the position vector of two arbitrary points on the panel(s). For the case of panels oriented conform with the underlying Cartesian coordinates, exact analytic results of this double surface integral are given in [5], allowing for an efficient numeric implementation. Calculation of the explicit result for the coefficient of potential can be made more robust against numerical instabilities by introducing virtual panels, cf. [16].

We assume that the electric coupling between two orthogonal segments is negligible compared to the case of parallel segments. With reference to Figure 1, the coil is partitioned into four multiconductor systems with N_c segments each, one multiconductor system for each side of the coil, which are combined for capacitance extraction. For the side of the coil where the bridge crosses the turns, there are $N_c = N_t + 2$ segments combined to a multiconductor system, whereas the other three sides each have $N_c = N_t$ segments combined. Thus, e.g., the coefficients of potential of any panel on one of the lateral surfaces of segments $\{1, 5, 9, 13, 14\}$ with any other panel on one of these segments are calculated and arranged in one matrix for each multiconductor system as

$$\mathbf{P} = \begin{pmatrix} \mathbf{P}_{11} & \mathbf{P}_{12} & \cdots & \mathbf{P}_{1N_c} \\ \vdots & & \ddots & \vdots \\ \mathbf{P}_{N_c1} & \mathbf{P}_{N_c2} & \cdots & \mathbf{P}_{N_cN_c} \end{pmatrix}. \quad (4)$$

Each $(N_p \times N_p)$ submatrix $\mathbf{P}_{k,l}$ contains the mutual coefficients of potential of all panels on the surface of segment k with all panels on the surface of segment l . The electrostatic potentials of the panels, stacked in column vector Φ_p , due to the free charges on the panels, stacked in column vector Q_p , are related as $Q_p = \mathbf{P}^{-1}\Phi_p$. Please note that the potentials in Φ_p are with respect to the infinite ground.

We are thus able to calculate the charges induced on a panel, if some of the panels are raised to a certain potential, say one Volt, while the other panels potentials are zero. We assume the four lateral areas of a segment to be equipotential surfaces. If one of the segments is raised to unit potential, vector Φ_p is zero everywhere apart from the all-ones vector at the position corresponding to this segment with raised potential, cf. [5]. Note that all panel charges Q_p on the segment with unit potential will be positive, whereas those on zero potential segments will be negative.

In a system with N_c conductors, the scalar capacitances (known to the circuit engineer) $C_{k,l}$ between conductors k and l are related to the conductors potentials Φ_k , Φ_l and charges

Q_k , Q_l as

$$\begin{aligned} Q_1 &= C_{10}\Phi_1 + C_{12}(\Phi_1 - \Phi_2) + \cdots + C_{1N_c}(\Phi_1 - \Phi_{N_c}) \\ Q_2 &= C_{21}(\Phi_2 - \Phi_1) + C_{20}\Phi_2 + \cdots + C_{2N_c}(\Phi_2 - \Phi_{N_c}) \\ &\vdots \\ Q_{N_c} &= C_{N_c1}(\Phi_{N_c} - \Phi_1) + C_{N_c2}(\Phi_{N_c} - \Phi_2) + \cdots + C_{N_c0}\Phi_{N_c}. \end{aligned} \quad (5)$$

Note that the capacitances are symmetric, i.e., $C_{k,l} = C_{l,k}$, and the zero potential Φ_0 is set to be zero. In order to solve this equation system, each of the conductors is sequentially raised to unit potential while all remaining ones are at zero potential, and the charges are determined.

From these observations, the scalar capacitances $C_{i,j}$ between two segments i and j are calculated by summing all negative panel charges from the corresponding segment i in vector Q_p when all panels on segment j are raised to unit potential, cf. [5]. The capacitance to the infinite ground C_{i0} is neglected in the following analysis, since we assume that there is no infinite reservoir of free charge acting as ground located in the coils proximity.

D. Equivalent Circuit Model

The partial resistances, inductances and capacitances are combined to a network as shown in Figure 2 for the subsequent mesh analysis. The capacitances are assigned to the coils corners with their values being determined by summing half of the capacitances of two neighboring segments (which may be separated by other parallel segments), e.g., C_2 in the figure is half the capacitance from segments 1-5 plus half the capacitance from segments 2-6. The first and the last capacitances C_1 and C_5 are given by the half segment capacitances 1-5 and 4-8. Since the coil in Figure 2 has only two turns, there are no further capacitances in the multiconductor system, as explained earlier. With more than 2 turns, there will also be capacitances in the corners connecting inner and outer turns. The capacitances of the bridge segment (that crosses all turns) to the underlying segments are assigned to the corner and the node where the bridge ends on the inner side of the coil, cf. C_6 in Figure 2. Note that limiting the capacitive current to flow only over the few nodes in the coils corner is an approximation, since more nodes would be necessary along each segment to model displacement currents more accurately. The division of segments into filaments is shown schematically for segment 1 in Figure 2 (the four parallel branches). In fact there are N_f branches, one for each filament, with a series resistance, self inductance and a controlled voltage source in parallel for each segment of the coil. The resistances and self inductances used for the subsequent mesh analysis are the values for the corresponding filament R_i and L_i . The value of the controlled voltage sources U_i in Figure 2 equals the sum of all mutual inductances to other parallel filaments $M_{i,j}$ multiplied by their currents and the complex angular frequency $\pm j\omega$, where the sign is determined by the current flow direction (positive for parallel and negative for antiparallel currents). The generator voltage source U_g used for the following mesh

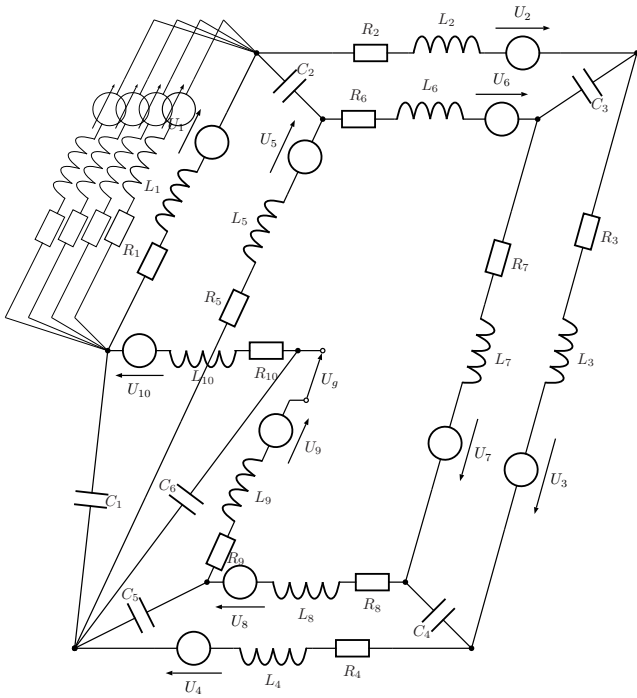


Figure 2. Equivalent circuit with lumped elements accounting for dominant field interactions. The elements are indexed with reference to Figure 1. The division of segments into filaments is shown schematically for segment 1 and in fact there are N_f parallel branches for each segment in this equivalent circuit (not shown).

analysis is assigned to the two nodes on the end of the last segment and the bridge, as shown in Figure 2.

E. Mesh Analysis

Standard mesh analysis is performed on the network as outlined in Figure 2. The systematic solution of the constitutional equations stated by Kirchhoff's voltage law requires the definition of tree and link branches. Each mesh equation is based on a loop consisting of a single link and arbitrary many tree elements. The link element defines the loops orientation. We choose an arbitrary filament in each segment to be the tree element. All other filament branches and the branches with the capacitances and the voltage source are thus link elements. The mesh incidence matrix \mathbf{M} is derived straight forward by filling $\{1, -1\}$ elements into an all zero matrix, depending on the relation of branch to loop orientation. The voltages across the branches and the currents flowing in the branches are stacked consecutively in vector \mathbf{U} and \mathbf{I} , respectively. The block diagonal impedance matrix is constructed as $\mathbf{Z}_b = \text{diag}(\mathbf{Z}_q, \mathbf{Z}_C, \mathbf{Z}_L)$, where \mathbf{Z}_q contains the scalar impedance of the voltage source, matrix \mathbf{Z}_C is diagonal with elements $\frac{1}{j\omega C}$ with corresponding capacitances C as introduced earlier, and matrix \mathbf{Z}_L contains the resistance and self inductance terms $R_i + j\omega L_i$ on its diagonal, and multiple block matrices with the filamentary mutual inductive coupling terms $\pm j\omega M_{i,j}$ of all the filaments in parallel segments.

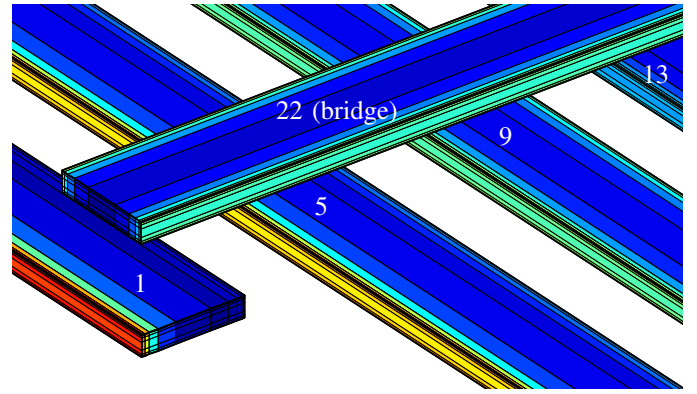


Figure 3. Current distribution at 10 MHz for segments in vicinity of the bridge for a coil with $N_t = 5$ turns. The colormap is derived from the maximum (red) and minimum (blue) current densities. The segments are labeled with reference to Figure 1. Skin and proximity effects are clearly visible.

The branch currents and voltages are calculated as

$$\mathbf{I} = -\mathbf{M}^T (\mathbf{M}\mathbf{Z}_b\mathbf{M}^T)^{-1} \mathbf{M}\mathbf{U}_q \quad (6)$$

$$\mathbf{U} = \mathbf{Z}_b\mathbf{I} + \mathbf{U}_q \quad (7)$$

where \mathbf{U}_q is the all zero column vector with only the first element containing the arbitrarily chosen applied source voltage U_g . The current and voltage of the first branch, the one containing the voltage source, relate the resulting coil impedance to $Z = \frac{U(1)}{I(1)}$. This impedance is compared to HFSS simulation results in the next section.

III. RESULTS AND COMPARISON TO HFSS SIMULATIONS

The geometry chosen for the coil simulation is aligned with the specifications for a Class 1 PICC coil according to ISO/IEC 14443-1 [12]. We would like to point out that typical aspect ratios of these coils lead to computationally expensive FEM simulations. With reference to Figure 1, the dimensions are chosen as $L = 80$ mm, $B = 48$ mm, $w = 0.25$ mm, $h = 0.05$ mm and $s = 0.15$ mm. The vertical gap between the bridge and the underlying segments is 0.5 mm and the number of turns is chosen as $N_t = 5$. The segments are assumed to be composed of copper with conductivity $\sigma = 58$ MS/m.

The lower and upper frequency limits used in the simulation are $f_{min} = 10$ MHz and $f_{max} = 70$ MHz. This results in a skin depth of $\delta_{max} = \sqrt{\frac{2}{2\pi f_{min}\mu\sigma}} \approx 21 \mu\text{m}$ at 10 MHz and $\delta_{min} = \sqrt{\frac{2}{2\pi f_{max}\mu\sigma}} \approx 7.9 \mu\text{m}$ at 70 MHz. The division of the segments into filaments, based on the method described in [13, p.97] with a skin factor $\chi = 2$ and following the $\delta/2$ rule, results in $N_w = 11$ and $N_h = 7$ and thus $N_f = 77$ filaments per segment. The lateral surfaces of the segments are divided into $P_l = 40$, $P_w = 3$ and $P_h = 1$ panels such that each lateral surface of a segment has a total of $N_p = 320$ panels. Figure 3 shows the relative current distribution simulated at 10 MHz for segments in vicinity to the bridge with segments labeled with reference to Figure 1. The colormap is derived from the maximum (red) and minimum (blue) current densities in the filaments of all segments. Current crowding due to both skin

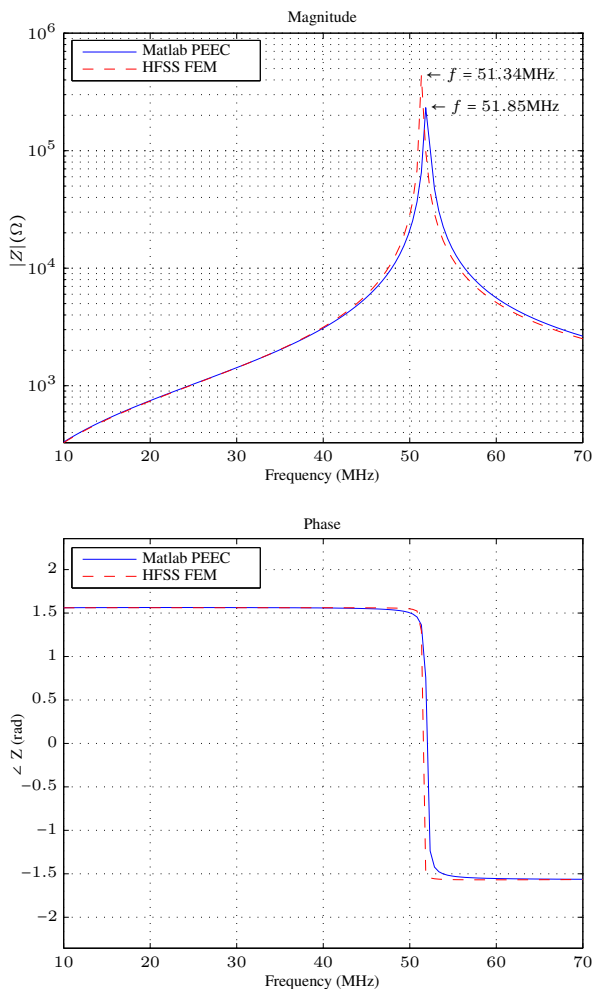


Figure 4. Magnitude and phase of coil impedance as a function of frequency comparing the presented PEEC method to HFSS FEM. The simulation methods show only a slightly different resonance frequency. The coil geometry is described in the text.

and proximity effects is clearly visible. Note that segment 9 in the figure is in the middle, with two turns on each side, such that the proximity effect nearly vanishes.

The impedance is calculated for a total of 120 equally spaced frequency points in the range $[f_{min}, f_{max}]$ and thus the step size is 0.5 MHz. Figure 4 illustrates the magnitude and phase of the PEEC coil impedance over frequency in comparison to HFSS FEM results. The first parallel resonance of the coil is well aligned in both simulations.

Both Matlab and HFSS FEM simulations were done on a 2.66 GHz Intel Dual Xeon X5650 (6 cores) with 24 GB RAM. Computation of the inductances (2) and coefficients of potential (3) was accelerated by making use of precompiled *.mex* functions and of Matlab parallel computing capabilities. Equation (6) was solved iteratively with a Generalized Minimum Residual (GMRES) method [17]. The first initial guess of the GMRES solution for the current frequency point was chosen from the solution obtained from the previous frequency

Table I
COMPARISON OF SIMULATION DURATION

	HFSS FEM	Matlab PEEC
Duration	2320 s	282 s

point (for the first simulation point, the initial guess is the default all zero vector).

The radiation boundary of the terminal driven HFSS FEM simulation was chosen as a sphere made of a perfect electric conductor. In HFSS, the mesh parameters were tuned such that the current distribution within the conductors was calculated with similar resolution in both simulations.

Both Matlab and HFSS distributed the simulation workload to multiple cores by making use of their parallel computing capabilities.

The simulation duration is shown in Table I. We were able to reduce the simulation duration by a factor of 8.2 with our Matlab tool based on the PEEC method. Further reduction of the simulation time for the PEEC method can be expected by solving equations (6) and (7) with methods such as the Fast Multipole Method or the Adaptive Cross Approximation method.

IV. CONCLUSION AND OUTLOOK

We have presented an efficient method for simulating a rectangular spiral coil based on the PEEC method using quasi-stationary results of the underlying mixed potential integral equation. An equivalent circuit accounting for dominant field interactions was introduced. The coil impedance, obtained by solving the mesh equations for this equivalent circuit, shows good alignment with the results obtained from HFSS FEM simulations over the frequency range of interest. Our Matlab tool excels at its low computational burden and ease of use and allows for optimization for various design goals.

ACKNOWLEDGMENTS

This work was funded by *Christian Doppler Laboratory for Wireless Technologies for Sustainable Mobility*, Module *Nearfield Power Efficiency* in collaboration with *NXP Semiconductors Austria GmbH*.

REFERENCES

- [1] T. Hubing, C. Su, H. Zeng, and H. Ke, "Survey of current computational electromagnetics techniques and software," *Technical Report: CVEL-08-011.2*, 2008.
- [2] R. Harrington, "Matrix methods for field problems," *Proceedings of the IEEE*, vol. 55, no. 2, pp. 136–149, feb. 1967.
- [3] C. Hoer and C. Love, "Exact inductance equations for rectangular conductors with applications to more complicated geometries," *Journal of Research of the National Bureau of Standards*, vol. 69, no. 2, pp. 127–137, 1965.
- [4] A. Ruehli, "Inductance calculations in a complex integrated circuit environment," *IBM Journal of Research and Development*, vol. 16, no. 5, pp. 470–481, 1972.
- [5] A. Ruehli and P. Brennan, "Efficient capacitance calculations for three-dimensional multiconductor systems," *IEEE Trans. Microw. Theory Tech.*, vol. 21, no. 2, pp. 76–82, 1973.
- [6] A. Ruehli, "Survey of computer-aided electrical analysis of integrated circuit interconnections," *IBM Journal of Research and Development*, vol. 23, no. 6, pp. 626–639, 1979.
- [7] K. Nabors and J. White, "Fastcap: A multipole accelerated 3-d capacitance extraction program," *IEEE Trans. Comput.-Aided Design Integr. Circuits Syst.*, vol. 10, no. 11, pp. 1447–1459, 1991.

- [8] M. Kamon, M. Tsuk, and J. White, "Fasthenry: A multipole-accelerated 3-d inductance extraction program," *IEEE Transactions on Microwave Theory and Techniques*, vol. 42, no. 9, pp. 1750–1758, 1994.
- [9] J. Garrett, A. Ruehli, and C. Paul, "Accuracy and stability improvements of integral equation models using the partial element equivalent circuit (peec) approach," *IEEE Transactions on Antennas and Propagation*, vol. 46, no. 12, pp. 1824–1832, 1998.
- [10] A. Ruehli, G. Antonini, J. Esch, J. Ekman, A. Mayo, and A. Orlandi, "Nonorthogonal peec formulation for time-and frequency-domain em and circuit modeling," *IEEE Trans. Electromagn. Compat.*, vol. 45, no. 2, pp. 167–176, 2003.
- [11] X. Hu, "Full-wave analysis of large conductor systems over substrate," Ph.D. dissertation, Massachusetts Institute of Technology, 2005.
- [12] "Identification cards - Contactless integrated circuit cards - Proximity cards - Part 1: Physical characteristics. Amendment 1: Additional PICC classes," International Standard ISO/IEC 14443-1, 05 2012.
- [13] P. Scholz, "Analysis and numerical modeling of inductively coupled antenna systems," Ph.D. dissertation, Theorie Elektromagnetischer Felder (TEMF), 2010.
- [14] A. Ruehli, "Equivalent circuit models for three-dimensional multiconductor systems," *IEEE Trans. Microw. Theory Tech.*, vol. 22, no. 3, pp. 216–221, 1974.
- [15] G. Zhong and C. Koh, "Exact closed-form formula for partial mutual inductances of rectangular conductors," *IEEE Trans. Circuits Syst. I*, vol. 50, no. 10, pp. 1349–1352, 2003.
- [16] J. Jain, C. Koh, and V. Balakrishnan, "Exact and numerically stable closed-form expressions for potential coefficients of rectangular conductors," *IEEE Trans. Circuits Syst. II*, vol. 53, no. 6, pp. 458–462, 2006.
- [17] Y. Saad and M. H. Schultz, "Gmres: A generalized minimal residual algorithm for solving nonsymmetric linear systems," *SIAM Journal on scientific and statistical computing*, vol. 7, no. 3, pp. 856–869, 1986.